Progress In Electromagnetics Research C, Vol. 107, 219–231, 2021

A Star-Wheel Design of Single Crystal Sapphire Optical Fiber Promoting Single Mode Operation in the Infrared Regime

Farhan Mumtaz[1, 2, 3, *], Yutang Dai[1, *], Muhammad A. Ashraf[3], and Wenbin Hu[1]

Abstract—In this study, a star-wheel design of single crystal sapphire optical fiber is proposed to achieve single mode operation in the infrared regime. In the azimuthal direction the structure retains a reduced core of higher refractive index. It is connected to the outer boundary via star-wheel configuration of segments. The region of alternating symmetrical truncated cavities of lower refractive index is air. The enclosed alternating layers of sapphire and air cavities around the reduced core function as cladding. Fiber structure in the azimuthal direction is uniformly distributed in the radial direction. Finite element method is employed to analyze the modal characteristics of fundamental and higher order modes. Under strongly guided approximation, the structure can effectively eliminate the large modal interference. The proposed waveguides, at operating wavelength of $\sim 1.55\,\mu$m, with the diameters of $\sim 50\,\mu$m, $75\,\mu$m, $100\,\mu$m, and $125\,\mu$m diameter, exhibit confinement loss of $\sim 0.0314\,$dB/m, $0.0072\,$dB/m, $0.0023\,$dB/m, and $0.0009\,$dB/m, respectively. It is anticipated that such a fiber can be a potential candidate in addressing a wide range of optical sensors and communication systems, which unable to sustain in extremely harsh environments. COMSOL multi-physics® is used to perform numerical investigations.

1. INTRODUCTION

Superlative material characteristics of single crystal sapphire optical fiber α-Al_2O_3 (SCF) offers various advantages, such as high resolution, superior rigidity, high laser power transfer, flexible strength, chemical unresponsiveness, optical spectroscopy, thermal shock resistance, and high melting point [1–4]. It is more sustainable and resistant than the ordinary silica fibers and can work under harsh environments [5–8]. An unclad SCF of a large core structure possesses large value of numerical aperture and effective refractive index, which turn the optical waveguide unrealistic in terms of reliability and compatibility. Such waveguides restrict numerous practical applications because of large modal interference, transmission losses, and contaminations. Efforts are made to design cladding for SCF by coating low refractive index surface layer, or deposition of highly reflective layer [9–11]. Such coating structures succeeded in the confinement of light propagation into core region of fiber. These fibers, when being exposed to extremely harsh environment loses thermal stability, caused by erosion of coated layer. Due to the lack of adequate cladding, SCF faces major challenges of contamination, reliability, and dopant diffusion, which hinders the performance and acceptance of such fibers in an optical industry.

Compared to silica fibers, the SCF exhibits wide operational range of temperature ~ 0 to 1800°C, hence, it is becoming a hot topic of research for different industrial units, i.e., gas turbines, coal gasifiers, and other extreme environment catalyst processes. SCF has diversified operating wavelength

Received 19 November 2020, Accepted 10 December 2020, Scheduled 18 December 2020

* Corresponding authors: Farhan Mumtaz (mfmawan@whut.edu.cn), Yutang Dai (daiyt6688@whut.edu.cn).

[1] National Engineering Laboratory for Fiber Optic Sensing Technology, Wuhan University of Technology, Luoshi Road 122#, Wuhan 430070, China. [2] School of Information and Communication Engineering, Wuhan University of Technology, Luoshi Road 122#, Wuhan 430070, China. [3] Communications Lab., Department of Electronics, Quaid-i-Azam University, Islamabad 45320, Pakistan.

range of 0.3 to 5 μm [12], enabling it to be used from ultra-violet (UV) to Terahertz (THz) wave-guiding. Nowadays, SCF is rapidly gaining popularity in interferometry, and numerous applications have been developed using SCF for interferometric sensing [13] and lasing [14]. SCF is multimode, and its smallest commercially available diameter is $\sim$ 75 μm and supports $\sim$ 23436 modes [15], still limits the fiber performance owing to large modal interference. Katyba et al. [16, 17] presented photonic crystal waveguides of hollow cores. They achieved low loss dispersion profile of SCF in THz regime and developed a circular geometry SCF close to 300 μm diameter for near field scanning probe microscopy. Nubling and Harrington [18] reported an SCF structure with low loss using laser-heated pedestal-growth method for the ultra violet and visible infrared wavelength regime. Hill et al. [19] presented single mode operation with a fiber diameter of 6.5 μm in the infrared wave-guiding regime by a post-fiber-growth chemical etching process. Cheng et al. [20, 21] explored by simulating a model of windmill shape SCF, to show that the confinement of single-mode is achievable with low loss by tailoring the "windmill" parameters at 532 nm of operating wavelength. This structure addresses the fundamental mode propagation over long distance, but in extreme case the handling of fringes like windmill structure is quite challenging. The structure does not have any appropriate cover. The fiber may face splintering of fringes. It can influence transmission deterioration possibly losing functioning in harsh environments. Recently in [1], our group has reported a precise hexagonal SCF waveguide of $\sim$ 35 micron radius that exhibits 0.077 dB/m confinement loss at 200 nm. Since the hexagonal SCF has a large radius, it supports a large number of modes, where a reduction in fiber diameter would make modal reduction possible, but it has limited range of operating wavelength.

To study FM confinement in the wide range of operating wavelength, a novel and effective design of SCF geometry is proposed. It is proposed that the effective core region is reduced by alternating symmetrical air cavities rounded with the segment of star-wheel configuration, such that alternating layers of higher and lower refractive indices are constituted angularly. The structure ensures the confinement of fundamental mode (FM) over long distance with low confinement loss (CL) and minimal dispersion. Higher order modes (HOMs) incorporate higher leakage loss, thus HOMs are strip-off, and clean single mode operation in the fiber is ensured. A rigorous analysis of segmented-cladding fiber by the radial-effective-index method [22] extends in the numerical investigations. The optical analysis of waveguides is extended up to 2.0 μm, and it is assumed that their results of optical losses, effective refractive index, and dispersion will be helpful for incorporating valuable contribution in the area of high-power fiber thulium and holmium lasers. As such, laser technology is evolving into a variety of optical applications. Accomplishment of such a fine SCF structure will also boost transmission efficiency, sensing capabilities, and thermal robustness, opening new corridors in the field of optical sensing and optics.

2. PROBLEM DESCRIPTION AND FORMULATION

2.1. Geometry of SCF

The transverse and longitudinal cross-section of proposed SCF is shown in Figs. 1(a) and (b), respectively, where transverse cross-section of SCF lies in the xy-plane; O is the origin; d_{out} is the SCF original diameter; d_{in} is the reduced diameter of effective core region; b is the width of outer boundary; m_1 and m_2 are the semi-minor and major-axes used to define the alternating segments of sapphire along with azimuthally distributed air cavities, as shown in Fig. 1(a). The proposed structure is uniform in radial direction, as shown in Fig. 1(b). The core and cladding refractive indices are n_1 and n_2, respectively. The cladding region is taken to be alternating angular array of high and low refractive indices. Free triangular meshing is defined for the proposed geometry to employ FEM. Using the predefined function of COMSOL MESH MENU, free triangular meshing sizes of "extra fine" and "normal" are calibrated for "sapphire" and "air" region, respectively. The perfect match layer (PML) of $\sim b/2$ is used in the simulations, as shown in Fig. 1(c). COMSOL MODE ANALYSIS is used to obtain the FM and HOM profiles of the structure, as shown in Figs. 1(d) and 1(e), respectively. In this study, four different samples are analyzed for numerical solutions, and their parameters of manufacturing are listed in Table 1. In addition, the proposed samples of SCF can be manufactured by different reported methods, such as edge-defined film-fed growth [23], laser-heated floating-zone directional solidification [24], laser-heated pedestal-growth [25], and micro pulling down [26].

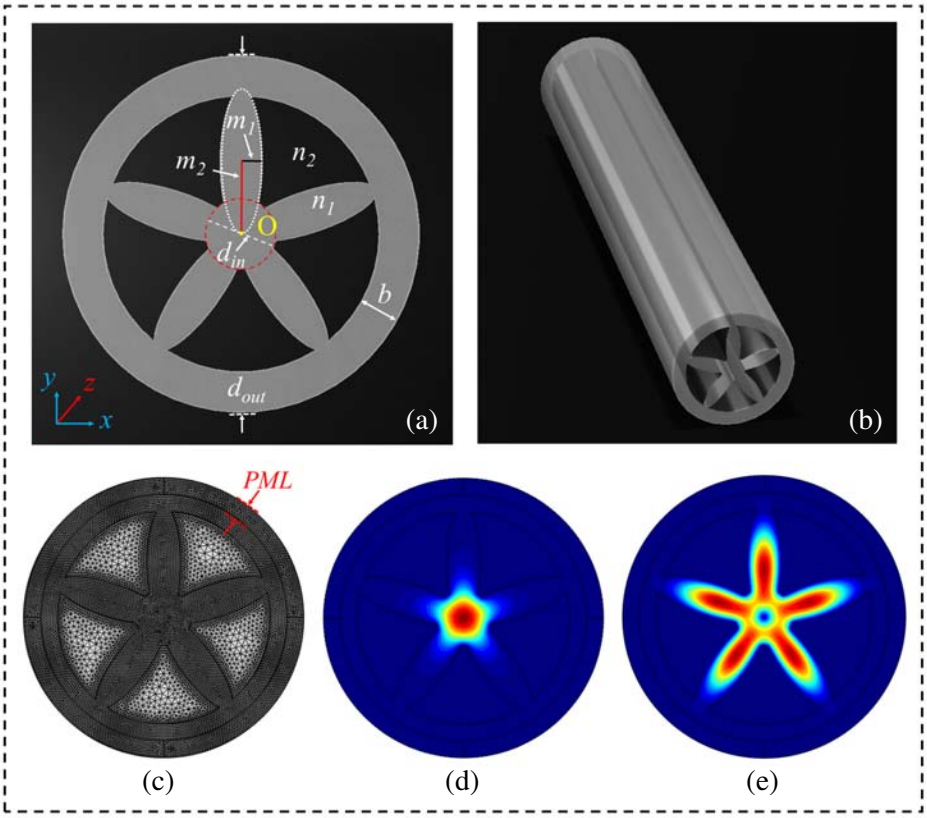

Figure 1. (a) Transverse, (b) longitudinal cross-section of the proposed SCF, (c) free triangular meshing by FEM solution, (d) fundamental mode, and (e) higher order mode profile.

Table 1. Fiber parameters for manufacturing.

Fiber Type	d_{out} (µm)	d_{in} (µm)	b (µm)	m_1 (µm)	m_2 (µm)	**PML** (µm)
SCF — 50 µm	50	10	6	3	20	3
SCF — 75 µm	75	15	9	4.5	30	4.5
SCF — 100 µm	100	20	12	6	40	6
SCF — 125 µm	125	25	15	7.5	50	7.5

2.2. Theoretical Formulation

In cylindrical coordinates system (r, ϕ, z), Maxwell's equations for electromagnetic fields in an optical waveguide of invariant index profile along the z-direction can be decomposed into transverse and longitudinal components as

$$\xi(r, \phi, z, t) = \{\xi_t(x, y) + \xi_z(x, y)\} \ e^{-j(\omega t - \beta z)}, \tag{1}$$

where ξ denotes the E or H field; subscripts t and z denote the transverse and longitudinal components, respectively; ω is the angular frequency; β is the complex propagation constant used to solve PML function in the computational domain. When electromagnetic wave reaches the boundary, PML boundary condition absorbs the electromagnetic waves with no reflection. Thus, light propagates in an ideal optical waveguide along z-direction. Maxwell's equations for an anisotropic-type of a PML

boundary condition can be expressed as [27],

$$\nabla \times E = -jk_o\mu_r [S] H, \tag{2}$$

$$\nabla \times H = jk_o\varepsilon_r [S] E, \tag{3}$$

and

$$[S] = \begin{bmatrix} S_x/S_y & 0 & 0 \\ 0 & S_x/S_y & 0 \\ 0 & 0 & S_xS_y \end{bmatrix}, \tag{4}$$

where $[S]$ is the PML matrix of 3×3, k_o the wave number in the vacuum, ε_r the relative dielectric permittivity, and μ_r the relative magnetic permittivity. Thereafter, FEM is employed which enables the modified eigen-mode values equation as [28, 29],

$$\nabla \times \mu_r^{-1} \left([S]^{-1} \nabla \times E \right) - k_0^2 \left(\varepsilon_r - \frac{j\sigma}{\omega} \right) [S] E = 0, \tag{5}$$

where

$$\gamma = k_0^2 \left(\varepsilon_r - \frac{j\sigma}{\omega} \right), \tag{6}$$

γ is the eigen-mode value, σ the electrical conductivity, and $[S]^{-1}$ the inverse of matrix $[S]$. The time harmonic electric field propagating out of plane can be expressed as,

$$E(x, y, z) = \mathrm{Re} \left[\tilde{E}(x, y) e^{j\omega t - \beta z} \right], \tag{7}$$

$\tilde{E}$ is the electric field phasor, and z is the direction of propagation,

$$\beta = k_o \mathrm{Re}(n_{eff}) + k_o \mathrm{Im}(n_{eff}) = -\gamma, \tag{8}$$

where $\mathrm{Re}(n_{eff})$ and $\mathrm{Im}(n_{eff})$ are the real and imaginary parts of β. The confinement loss (CL) can be calculated as [30–32]

$$\mathrm{CL} = 8.868 k_o \mathrm{Im}(n_{eff}), \tag{9}$$

Further, the dispersion relation of an optical waveguide can be estimated as [32],

$$\mathrm{D} = -\frac{\lambda}{c} \frac{d\left(\mathrm{Re}(n_{eff})\right)}{d\lambda^2} \tag{10}$$

3. NUMERICAL RESULTS AND DISCUSSION

In order to demonstrate modal reduction, a star-wheel design of SCF structure is proposed. The star-wheel structure varies azimuthally and radially, and it is uniform. The large core of SCF can be effectively reduced by introducing the symmetrical air cavities. Alternating high and low refractive region around the reduced core can be constituted. This region is cladding region. The refractive index of the sapphire and air region used in the numerical investigation are $n_1 = 1.7462$ and $n_2 = 1$, respectively. The operating wavelength of 1.5 µm is used for simulation.

3.1. Electric Field Distribution

COMSOL multi-physics® software is employed to perform the modal analysis. The spectral wavelength range of 0.3–2.0 µm is used for modal analysis. From Eq. (6), FEM is used to obtain the modified eigen-mode value through the built-in function of free triangular meshing, as shown in Fig. 1(c). Multiple iterations are performed until the solution converges to a defined error limit. Electric field (E-field) distributions of FM and HOM for proposed geometry are obtained by employing the PML, as defined by the PML matrix $[S]$ from Eqs. (4) and (5). The obtained E-fields at 0.3 µm and 1.55 µm for FM and HOM are shown in Figs. 2(a) and (b), respectively. It can be inferred from Figs. 2(a)–(b) that counter profile seems analogous but their differential ratio in the case of HOM is inconsistent at lower and higher wavelengths. The trend for the confinement of FM deemed obvious at both operating wavelengths. However, the HOM generates strong evanescent field, which may contribute to higher leakage loss.

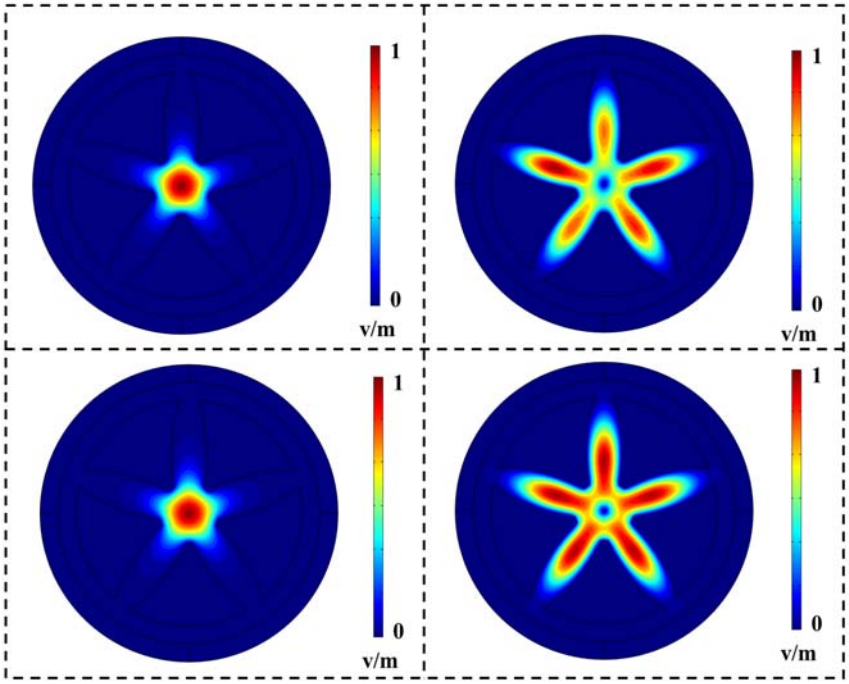

Figure 2. Simulated normalized E-field distribution of (a) FM (top $\sim \lambda = 0.3\,\mu m$ and bottom $\sim \lambda = 1.5\,\mu m$, (b) HOM (top $\sim \lambda = 0.3\,\mu m$ and bottom $\sim \lambda = 1.5\,\mu m$).

3.2. Confinement Loss and Effective Refractive Index

In order to investigate the leakage loss of FM and HOM, the CL is inspected at different wavelengths, i.e., from 0.3 µm to 2.0 µm. CL strongly depends on imaginary part of effective refractive index, and its values corresponding to given geometry are obtained from Eq. (9). The proposed SCF with different diameters, i.e., 50 µm, 75 µm, 100 µm, and 125 µm, exhibits CL of 0.0314 dB/m, 0.0072 dB/m, 0.0023 dB/m, and 0.0009 dB/m, respectively, at the operating wavelength of 1.55 µm. The absolute values of CL for

Table 2. Confinement loss and effective refractive index as a function of wavelength.

Wavelength (µm)		$\lambda =$ **0.3**		$\lambda =$ **0.8**		$\lambda =$ **1.55**		$\lambda =$ **2.0**	
	Diameter (µm)	**FM**	**HOM**	**FM**	**HOM**	**FM**	**HOM**	**FM**	**HOM**
CL (dB/m)	50	3.31×10^{-4}	2.7348	0.00509	17.103	0.03142	40.015	0.057104	59.511
	75	8.64×10^{-5}	0.85839	0.00105	8.8647	0.00728	15.337	0.013986	21.065
	100	3.45×10^{-5}	0.38455	3.65×10^{-4}	2.4471	0.00238	8.3557	0.004823	10.917
	125	1.71×10^{-5}	0.20774	1.66×10^{-4}	1.2618	9.92×10^{-4}	6.4716	0.002017	6.8201
$\mathbf{n}_{eff}$	50	1.8143	1.8142	1.7594	1.7597	1.7435	1.7411	1.7341	1.7304
	75	1.8143	1.8143	1.7598	1.7595	1.7449	1.7438	1.7364	1.7347
	100	1.8143	1.8143	1.7599	1.7598	1.7455	1.7448	1.7372	1.7362
	125	1.8143	1.8143	1.76	1.7599	1.7457	1.7453	1.7376	1.737

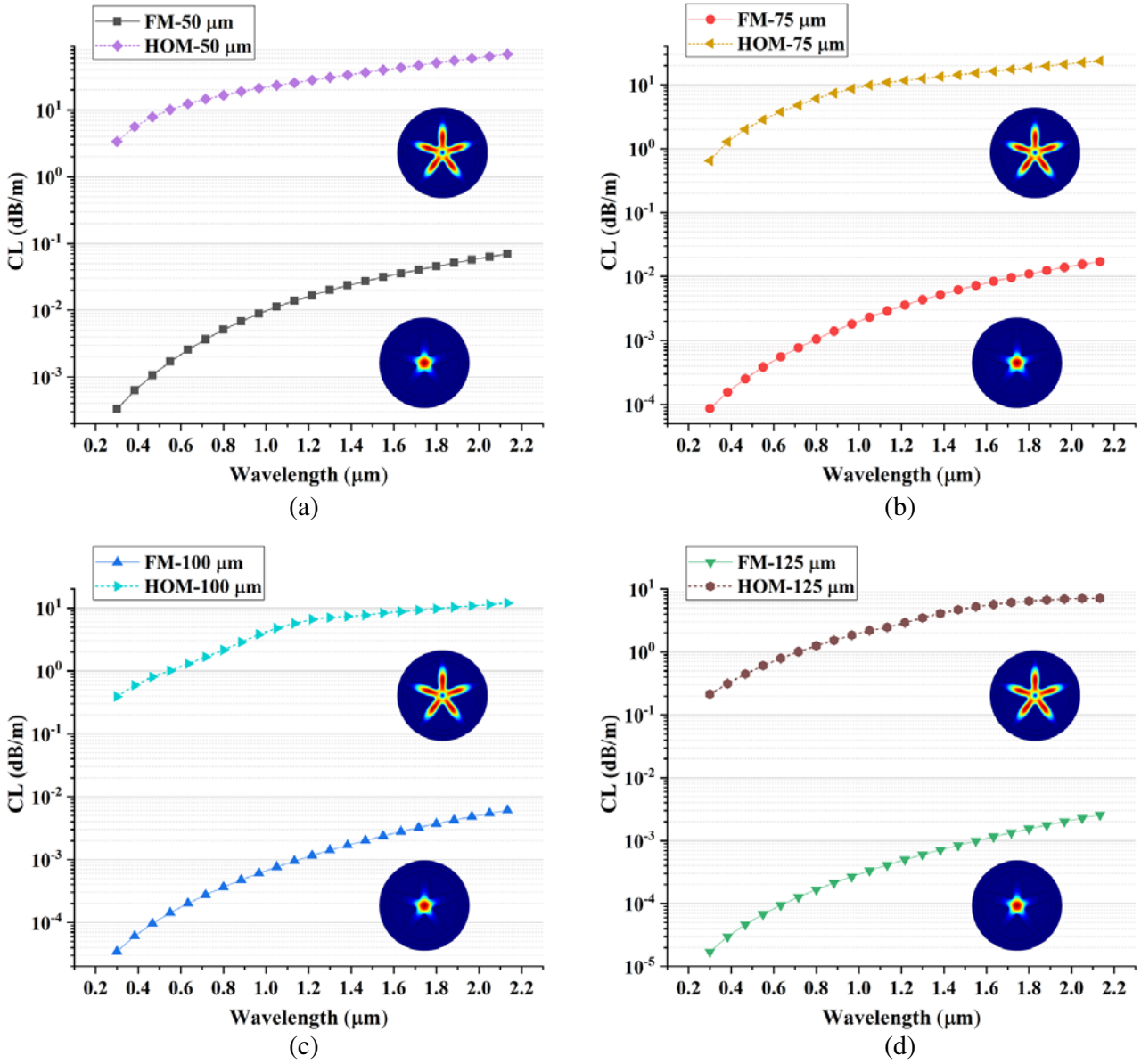

Figure 3. CL as a function of wavelength for different diameter of SCF, (a) 50 μm, (b) 75 μm, (c) 100 μm, and (d) 125 μm.

different diameters of fiber show that the proposed geometry ensures the propagation of FM with low CL. On the other hand, the HOM presents high leakage loss with differential loss factor of 10^3 to 10^4 dB/m. These modes can be easily stripped off from fiber over the shortest propagation distance, i.e., less than 1 meter. The graphical summary of CL for different proposed diameters of the SCF geometry in comparison with FM and HOM as a function of wavelength from 0.3 μm to 2.0 μm is given in Figs. 3(a)–(d). The effective refractive index of the proposed SCF is also numerically calculated by Sellmeier equation [1], and a comparison is made by varying the operating wavelength. From Figs. 4(a)–(d), the graphic summary elucidates the variation of n_{eff} as a function of wavelength. The insets of each figure describe the n_{eff} difference of FM and HOM with a comparison of real sapphire refractive index. The detailed numerical results of CL and n_{eff} at different wavelengths of 0.3 μm, 0.8 μm, 1.55 μm, and 2.0 μm are listed in Table 2.

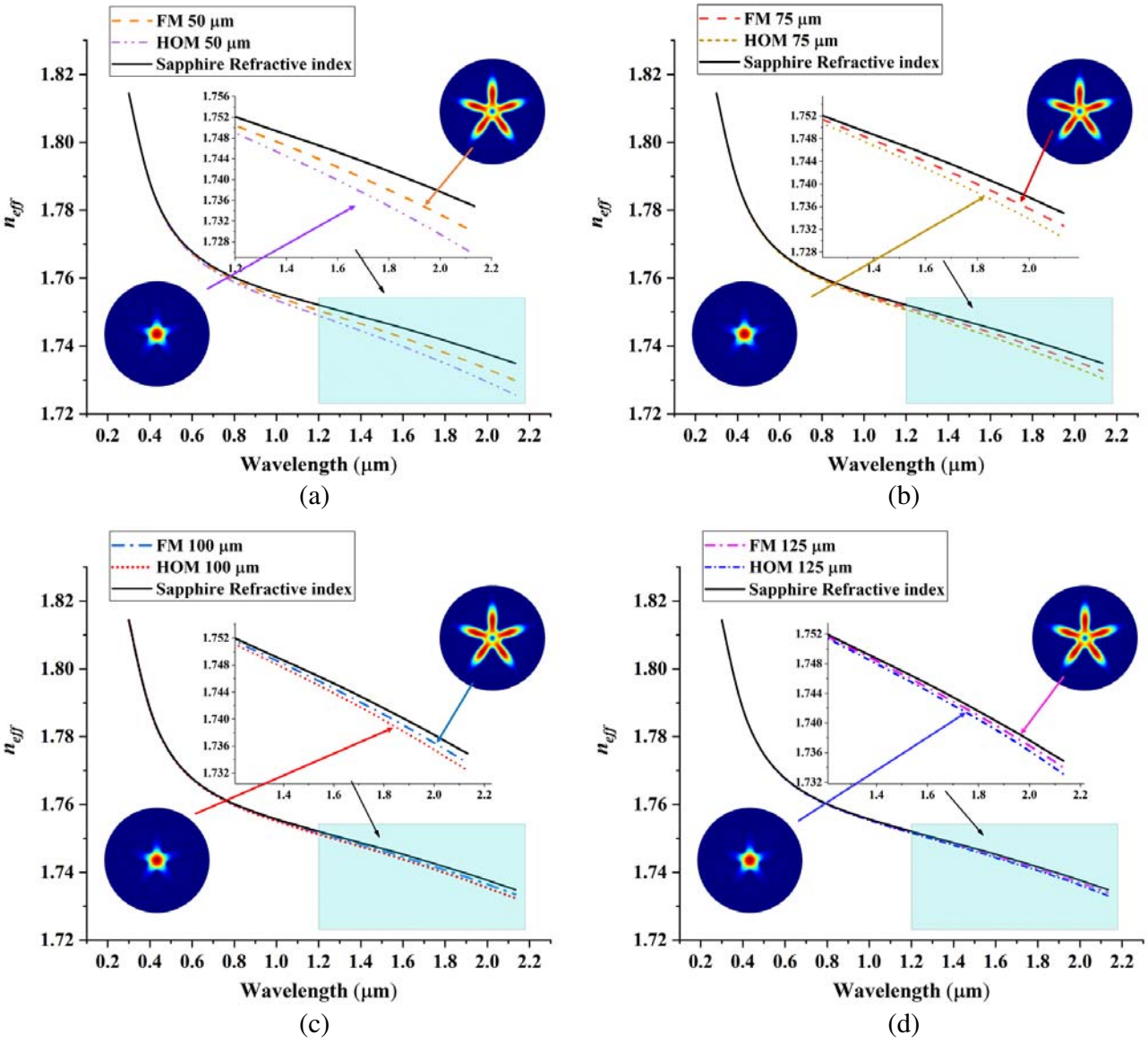

Figure 4. The variation of effective refractive index n_{eff} of proposed SCF as a function of wavelength in comparison with Sapphire refractive index; for different diameters, (a) 50 µm, (b) 75 µm, (c) 100 µm and (d) 125 µm.

3.3. Chromatic Dispersion

The chromatic dispersion of proposed samples of SCF at the operating wavelengths in between 0.3 µm and 2.0 µm is shown in Fig. 5. It can be inferred from dispersion curves that the proposed SCF exhibits ultra-flattened, nearly zero chromatic dispersion over the observed wavelength in between 1.1 and 1.6 µm. In the range of near and short wavelength of infrared bands, dispersion variation of 4.2 ps/(nm · km) is observed, which is given in the inset of Fig. 5. However, when the wavelength is increased from 1.6 µm to 2.0 µm, the fiber posed slightly dispersive from 33 to 117 ps/(nm · km). A comparison of chromatic dispersion corresponding to FM of SCF with material dispersion of sapphire is numerically evaluated from Eq. (10), and their results are listed in Table 3.

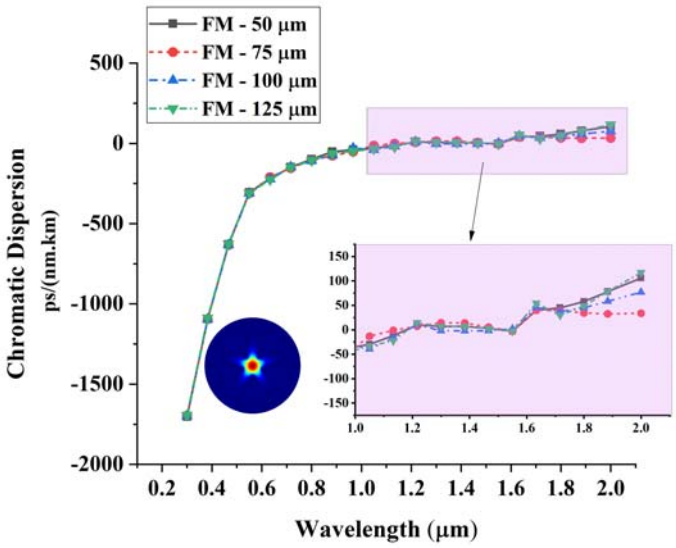

Figure 5. Chromatic dispersion as a function of wavelength.

Table 3. Chromatic dispersion as a function of wavelength.

Wavelength (µm)		$\lambda =$ **0.3**	$\lambda =$ **0.8**	$\lambda =$ **1.55**	$\lambda =$ **2.0**
	Diameter (µm)	**FM**	**FM**	**FM**	**FM**
Chromatic dispersion (ps/nm · km)	50	−1703.55	−98.35	−3.04	105.76
	75	−1695.89	−103.85	−2.90	33.71
	100	−1698.41	−107.51	1.96	77.06
	125	−1692.75	−105.68	−2.60	117.05
Material dispersion in Sapphire	-	−5108.6	−170.82	25.50	57.316

3.4. Mode Field Radius (MFR) and Numerical Aperture (NA)

In order to analyze the optical properties of the SCF involving mode field analysis and numerical aperture (NA), FEM is utilized to solve the radial effective index that was used for analyzing any step index fibers, photonic crystal fibers, and other special structures. Since analytical solution of real and imaginary propagation constants is quite cucumber to solve, as given in Eq. (8), numerical solution of FEM is employed. The mode field radius (MFR) and *NA* are numerically solved, as effective area is 2×

Table 4. Numerical aperture and mode field diameter of proposed fiber.

Fiber type	**Numerical aperture(NA)**				**MFD (µm)**
	$\lambda =$ **0.3** (µm)	$\lambda =$ **0.8** µm	$\lambda =$ **1.55** µm	$\lambda =$ **2.0** µm	
SCF — 50 µm	0.0190491	0.0496352	0.097068	0.1221955	13
SCF — 75 µm	0.0190491	0.0324957	0.0647259	0.0833643	18
SCF — 100 µm	0.0190491	0.026533	0.0494387	0.0645811	24
SCF — 125 µm	0.0190491	0.0187619	0.0417846	0.0527333	26

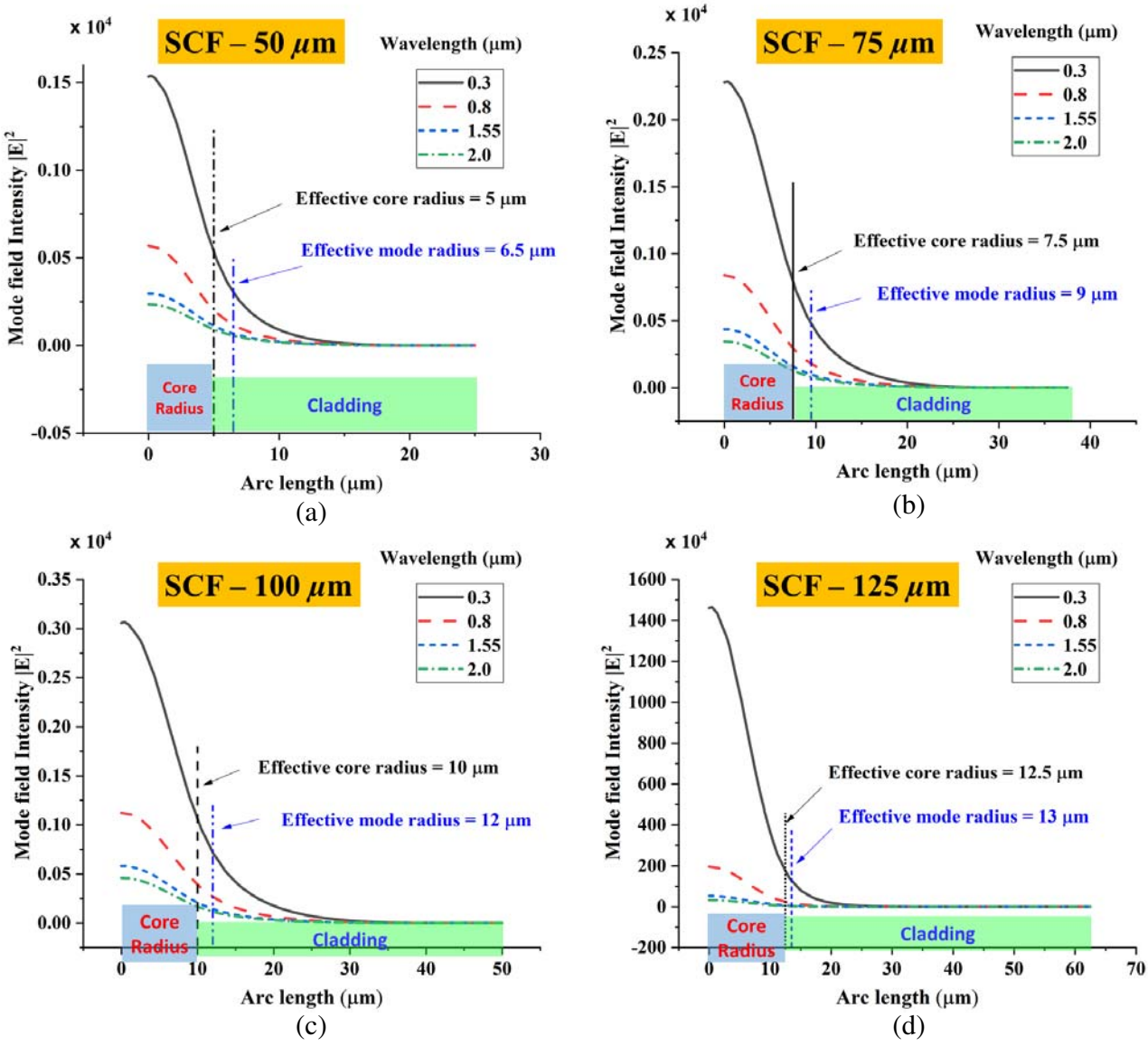

Figure 6. The evolution of mode field radius via intensity profile of FM, which is formulated in comparison with effective core radius for different diameters of proposed SCFs, (a) 50 μm, (b) 75 μm, (c) 100 μm and (d) 125 μm.

times of an order of MFR that is used to define mode field diameter (MFD) and determines the power field density. As we can see from the summary, Fig. 6, intensity profile of FM shows that smaller MFR would anticipate higher nonlinear effects on incidence, whereas NA of an angularly segmented cladding can be defined by replacing n_2 with n_{eff} [33], thus $NA = \sqrt{n_1^2 - n_{eff}^2}$, and its plot as a function of wavelength is shown in Fig. 7. MFD and NA of the fiber are numerically evaluated as a function of fiber arc length and operating wavelength, respectively, and their results are listed in Table 4.

3.5. Guided Mode Analysis

The number of guided modes in a fiber is obtained by solving Helmholtz equation with appropriate boundary conditions. An ordinary single-mode optical fiber ensures single-mode operation under weakly guided approximations ($n_1 \approx n_2$). Single-mode operation in an optical fiber is only possible if $V < 2.405$,

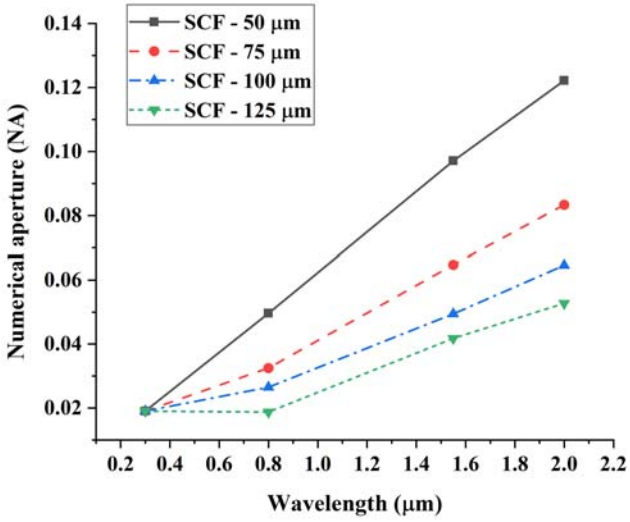

Figure 7. *NA* as a function of wavelength.

and the parameter V for an optical waveguide can be estimated as [34],

$$V = \pi \frac{d}{\lambda} \sqrt{n_1^2 - n_2^2} \tag{11}$$

where d is the core diameter, λ the operating wavelength, and the number of guided modes for a large core optical fiber can be estimated as [20]

$$M = \frac{4}{\pi^2} V^2 \tag{12}$$

The number of guided modes in a conventional SCF with reduced diameter of fiber is given by Eq. (12). The graphical analysis of M for a conventional SCF in comparison with proposed SCF is given in Fig. 8. It can be inferred from the summary that a large number of guided modes propagate in a conventional SCF. This can be decreased by the reduction of core size, but still large modal interference exists. In contrast, the use of segmented cladding (star-wheel shape) in SCF geometry has significantly

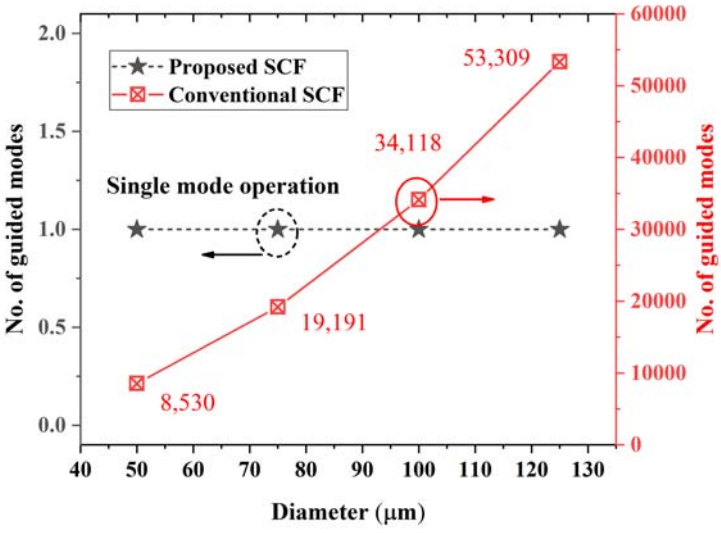

Figure 8. Comparison of number of guided mode in conventional SCF with proposed SCF.

reduced CL and chromatic dispersion, whereas HOM exhibits higher leakage loss with differential loss factor of 10^3 to 10^4 dB/m than FM. Ultra-flatten dispersion slope in the infrared regime ensures single mode operation for the proposed SCF samples of 50 µm, 75 µm, 100 µm, and 125 µm. Thus, it is fully capable of maintaining single mode operation. Compared with the CL of conventional SCF $\sim 10^6$ dB/m [21], the proposed SCF exhibits negligible CL, which is $\sim 10^{-3}$ to 10^{-4} dB/m. Considering the simulate performance, it is proposed that the star-wheel design of SCF is reliable and sustainable candidate in the harsh and extremely high-temperature environments. Also, this structure can suppress large modal interference and gives single mode operation with low CL and minimal chromatic dispersion.

4. CONCLUSION

A novel design of star-wheel shape of SCF with single mode operation in the spectrum of ultraviolet to short infrared wavelength is demonstrated. The structure retains a reduced core region surrounded by alternating segmented cladding region in the azimuthal directions, whereas radially fiber remains uniform. The effect of segmented cladding with the variation of four different fiber diameters is investigated. FEM analysis successfully demonstrates that differential loss factor of CL for HOM is $\sim 10^4$ times greater than FM, thereafter fiber ensuring clean single mode operation. FM of the waveguides exhibits low confinement loss of $\sim$ 0.0314, 0.0072, 0.0023, and 0.0009 dB/m and minimal chromatic dispersion of ~ -3.04, -2.90, 1.96, and -2.60 ps/(nm $\cdot$ km), for 50 µm, 75 µm, 100 µm, and 125 µm diameter, respectively at operating wavelength of $\sim$ 1.55 µm. Numerical results demonstrate that the proposed SCF can promote its application in wide range of interferometry and optics in extremely harsh environments.

REFERENCES

1. Mumtaz, F., M. A. Ashraf, Y. Dai, and W. Hu, "Numerical solution of strongly guided modes propagating in sapphire crystal fibers (α-Al_2O_3) for UV, VIS/IR wave-guiding," *Results in Physics*, Vol. 18, 103311, Sep. 2020.
2. Katyba, G. M., K. I. Zaytsev, I. N. Dolganova, I. A. Shikunova, N. V. Chernomyrdin, S. O. Yurchenko, G. A. Komandin, I. V. Reshetov, V. V. Nesvizhevsky, and V. N. Kurlov, "Sapphire shaped crystals for waveguiding, sensing and exposure applications," *Progress in Crystal Growth and Characterization of Materials*, Vol. 64, No. 4, 133–151, Dec. 2018.
3. Chen, H., K. Liu, Y. Ma, F. Tian, and H. Du, "Nanostructured sapphire optical fiber for sensing in harsh environments," *Micro-and Nanotechnology Sensors, Systems, and Applications IX*, Vol. 10194, 101941P, International Society for Optics and Photonics, May 18, 2017.
4. Bera, S., B. Liu, J. Wuenschell, J. Baltrus, D. Lau, B. Howard, M. Buric, B. Chorpening, and P. Ohodnicki, "Fabrication and evaluation of sapphire fiber cladding via magnesium aluminate spinel sol-gel based approaches," *Fiber Optic Sensors and Applications XVI*, Vol. 11000, 110000J, International Society for Optics and Photonics, May 14, 2019.
5. Buric, M., B. Liu, J. Thapa, and B. Chorpening, "Single-crystal fiber structures for harsh environment applications (Rising Researcher Presentation)," *Fiber Optic Sensors and Applications XV*, Vol. 10654, 106540N, International Society for Optics and Photonics, May 14, 2018.
6. Ohanian, III, O. J., A. J. Boulanger, S. D. Rountree, J. T. Jones, A. Birri, and T. E. Blue, "Single-mode sapphire fiber optic distributed sensing for extreme environments, *Micro-and Nanotechnology Sensors, Systems, and Applications XI*, Vol. 10982, 109822N, International Society for Optics and Photonics, May 13, 2019.
7. Pfeiffenberger, N., G. Pickrell, K. Kokal, and A. Wang, "Sapphire photonic crystal fibers," *Optical Engineering*, Vol. 49, No. 9, 090501, Sep. 2010.
8. Wang, T., J. Zhang, N. Zhang, S. Wang, B. Wu, N. Lin, P. Kusalik, Z. Jia, and X. Tao, "Single crystal fibers: Diversified functional crystal material," *Advanced Fiber Materials*, 1–25, 2019.
9. Spratt, W., M. Huang, T. Murray, and H. Xia, "Optical mode confinement and selection in single-crystal sapphire fibers by formation of nanometer scale cavities with hydrogen ion implantation," *Journal of Applied Physics*, Vol. 114, No. 20, 203501, Nov. 2, 2013.

10. Shen, Y., L. Tong, and S. Chen, "Performance stability of the sapphire fiber and cladding under high temperature," *Harsh Environment Sensors II*, Vol. 3852, 134–142, International Society for Optics and Photonics, Dec. 8, 1999.
11. Wilson, B. A., C. M. Petrie, and T. E. Blue, "High-temperature effects on the light transmission through sapphire optical fiber," *Journal of the American Ceramic Society*, Vol. 101, No. 8, 3452–3459, Aug. 2018.
12. Chen, H., M. Buric, P. R. Ohodnicki, J. Nakano, B. Liu, and B. T. Chorpening, "Review and perspective: Sapphire optical fiber cladding development for harsh environment sensing," *Applied Physics Reviews*, Vol. 5, No. 1, 011102, Mar. 2018.
13. Zhu, Y., Z. Huang, F. Shen, and A. Wang, "Sapphire-fiber-based white-light interferometric sensor for high-temperature measurements," *Optics Letters*, Vol. 30, No. 7, 711, 2005.
14. Wang, S.-C., C.-Y. Hsu, T.-T. Yang, D.-Y. Jheng, T.-I. Yang, T.-S. Ho, and S.-L. Huang, "Laser-diode pumped glass-clad Ti:sapphire crystal fiber laser," *Optics Letters*, Vol. 41, No. 14, 3217, 2016.
15. Djeu, N., see http://www.micromaterialsinc.com for pioneer commercial sapphire fiber provider.
16. Katyba, G. M., N. V. Chernomyrdin, I. N. Dolganova, A. A. Pronin, I. V. Minin, O. V. Minin, K. I. Zaytsev, and V. N. Kurlov, "Step-index sapphire fiber and its application in a terahertz near-field microscopy," *Proc. SPIE 11164, Millimetre Wave and Terahertz Sensors and Technology XII*, 111640G, Oct. 18, 2019.
17. Katyba, G. M., K. I. Zaytsev, N. V. Chernomyrdin, I. A. Shikunova, G. A. Komandin, V. B. Anzin, and M. Skorobogatiy, "Sapphire photonic crystal waveguides for terahertz sensing in aggressive environments," *Advanced Optical Materials*, 1800573, 2018.
18. Nubling, R. K. and J. A. Harrington, "Optical properties of single-crystal sapphire fibers," *Applied Optics*, Vol. 36, No. 24, 5934–5940, Aug. 20, 1997.
19. Hill, C., D. Homa, Z. Yu, Y. Cheng, B. Liu, A. Wang, and G. Pickrell, "Single mode air-clad single crystal sapphire optical fiber," *Applied Sciences*, Vol. 7, No. 5, 473, May 2017.
20. Cheng, Y., C. Hill, B. Liu, Z. Yu, H. Xuan, D. Homa, A. Wang, and G. Pickrell, "Design and analysis oflarge-core single-mode windmill single crystal sapphire optical fiber," *Optical Engineering*, Vol. 55, No. 6, 066101, Jun. 1, 2016.
21. Cheng, Y., C. Hill, B. Liu, Z. Yu, H. Xuan, D. Homa, A. Wang, and G. Pickrell, "Modal reduction in single crystal sapphire optical fiber," *Optical Engineering*, Vol. 54, No. 10, 107103, Oct. 2015.
22. Rastogi, V. and K. S. Chiang, "Analysis of segmented-cladding fiber by the radial-effective-index method," *JOSA B*, Vol. 21, No. 2, 258–265, Feb. 1, 2004.
23. LaBelle, Jr, H. E., "EFG, the invention and application to sapphire growth," *Journal of Crystal Growth*, Vol. 50, No. 1, 8–17, Sep. 1, 1980.
24. Mesa, M. C., P. B. Oliete, V. M. Orera, J. Y. Pastor, A. Martín, and J. Llorca, "Microstructure and mechanical properties of $Al_2O_3/Er_3Al_5O_{12}$ eutectic rods grown by the laser-heated floating zone method," *Journal of the European Ceramic Society*, Vol. 31, No. 7, 1241–1250, Jun. 1, 2011.
25. Andreeta, E. R., M. R. Andreeta, and A. C. Hernandes, "Laser heated pedestal growth of $Al_2O_3/GdAlO_3$ eutectic fibers," *Journal of Crystal Growth*, Vol. 234, No. 4, 782–785, Feb. 1, 2002.
26. Yoshikawa, A. and V. Chani, "Growth of optical crystals by the micro-pulling-down method," *MRS Bulletin*, Vol. 34, No. 4, 266–270, Apr. 2009.
27. Cherin, A. H., An Introduction to Optical Fiber, McGraw-Hill Inc, 1987.
28. Jia, C., N. Wang, K. Li, and H. Jia, "Dual-cladding high birefringence photonic crystal fiber with elliptical-core," *Applied Physics B*, Vol. 125, No. 9, 158, Sep. 2019.
29. Burman, E., D. Elfverson, P. Hansbo, M. G. Larson, and K. Larsson, "Shape optimization using the cut finite element method," *Comput. Methods Appl. Mech. Engrg.*, Vol. 328, 242–261, 2017.
30. Hossain, M. B., A. A. Bulbul, M. A. Mukit, and E. Podder, "Analysis of optical properties for square, circular and hexagonal photonic crystal fiber," *Optics and Photonics Journal*, Vol. 7, No. 11, 235–243, Nov. 2017.

31. Biswas, S. K., M. I. Hasan, M. A. Awsaf, M. N. Rahman, M. I. Abdullah, and M. M. Mia, "Design and analysis of hexagonal photonic crystal fiber with ultra-high birefringent and large negative dispersion coefficient for the application of sensing and broadband dispersion compensating fiber," *Asian Journal of Applied Science and Technology (AJAST)*, Vol. 1, No. 8, 147–151, Sep. 2017.
32. Begum, F. and P. E. Abas, "Near infrared supercontinuum generation in silica based photonic crystal fiber," *Progress In Electromagnetics Research C*, Vol. 89, 149–159, 2019.
33. Millo, A., I. Naeh, Y. Lavi, and A. Katzir, "Silver-halide segmented cladding fibers for the middle infrared," *Applied Physics Letters*, Vol. 88, No. 25, 251101, 2006.
34. Dutta, A., "Mode analysis of different step index optical fibers at 1064 nm for high power fiber laser and amplifier," *OSF Preprints*, Oct. 18, 2019.